Receding-horizon optimization of unbalanced distribution systems with time-scale separation for discrete and continuous control devices

Nawaf Nazir   Mads Almassalkhi
Department of Electrical and Biomedical Engineering
University of Vermont
Burlington, USA
{mnazir, malmassa}@uvm.edu

Abstract—This paper presents a method for the optimal control of discrete and continuous devices in an unbalanced three-phase distribution network with significant renewable generation. A hierarchical control scheme is presented where the discrete mechanical assets are dispatched at a slow time-scale as a mixed-integer program (MIP) and the continuous DERs are controlled at a fast time-scale as a convex program. The optimization programs are operated at two time scales as they manage controllable grid resources with different levels of responsiveness and flexibility. The MIP optimizes slow mechanical assets to position voltage robustly against uncertain net-load and a three-phase SOCP program is used to solve the fast loss-minimization optimization for the continuously operated DERs while providing corrective control against the intermittent and variable renewable net-load generation. The scheme is presented on the IEEE-13 node test feeder.

Index Terms—Distributed energy resources, distribution system optimization, energy storage, loss minimization, voltage regulation.

I. INTRODUCTION

The rapid growth in renewable generation over the past decade has underscored the importance of large-scale integration of feeder and substation automation technologies, energy storage, demand response, and energy management programs [1], [2]. With the energy flexibility inherent to many DERs, future grid operational paradigms must dispatch them to engender and maintain optimal network conditions, even under significant renewable (but intermittent) generation. The optimal power flow (OPF) is a useful tool to coordinate the grid resources subject to power balance constraints. Traditionally, *DistFlow* algorithms based on *branch flow power models* are used to solve the OPF problem in distribution networks [3]. However, these methods assume a balanced network model, which is not the case when 3-phase distribution networks with significant small-scale renewable generation are considered. Distribution systems are often unbalanced and it becomes necessary to study the three-phase model of the system for

accurate analysis and control [4]. The distribution grid is also made up of many different types of discrete and continuous operated devices. These devices operate at different time scales, which necessitates the use of separate optimization loops to coordinate them. Furthermore, the mechanical assets also have operational constraints on tap changes per hour to limit wear and tear, which necessitates separation. Heuristics have been proposed to solve this problem, but given the large number of devices encountered in practical systems, they represent a computational challenge [5]. The flexibility offered by inverter-based energy storage devices can make them an integral part of distribution system operations. In fact, optimized energy storage dispatch will play an important role in cost-effective integration of solar PV with grid operations [6]. However, the addition of storage leads to the coupling of different time-steps, which complicates the OPF models. This requires solving a multi-period optimization problem based on the prediction of load and solar generation.

The power flow equations relate the voltages in the network with the power injections. The solution space of the power flow equations is generally non-convex due to their non-linear nature [7]. The aim of the optimal power flow (OPF) problem is to attain certain distribution system objectives while satisfying all the network and device constraints. Recently, there have been efforts to use convex optimization techniques to solve the OPF problem [8], [9]. Previous works in literature have shown that for certain (e.g. radial) network topologies, the convex relaxations, such as second order cone programs (SOCP) and SDP can be exact [10], [11]. In [8] the necessary and sufficient conditions for a zero duality gap, i.e., the primal and dual solutions have the same optimal value, is given. It is shown that the zero duality gap holds for many practical IEEE systems after adding resistance to every transformer and when load over-satisfaction is allowed. However, these methods only deal with the balanced single phase equivalent models. Furthermore, SDP solvers are still not numerically robust [12].

Linear approximate models can also be powerful when they are sufficiently accurate. One particular approximation is an extension of the *DistFlow* model to three-phase unbalanced

power flows, *Dist3Flow*, that is obtained by linearization and certain assumptions on the per-phase imbalances [13], [14]. Discrete devices like the capacitor/reactor banks and line regulators (ON/OFF) and load-tap-changing (LTC) transformers are an integral part of the distribution management system. Due to the discrete state of these devices, including them into an optimization problem renders the problem NP-hard [15]. Previously, McCormick relaxation and linearization techniques have been used to incorporate these devices into the OPF problem for a balanced network [16]. This paper builds upon these works but leverages the notion that discrete devices and continuous DERs can offer their flexibility at different timescales and, hence, can be optimized in separate loops.

Distribution networks are inherently unbalanced which makes it necessary to study the full three-phase models of these networks. In [17], [18] the authors use SDP rank constraint relaxation to the three phase model of a distribution network. However, the inclusion of storage devices' state-of-charge (integrator) dynamics require multi-period optimization. The authors in [19], [20] have used multi-period SDP relaxation techniques to solve this problem in transmission networks, whereas in [21], the authors have utilized an AC-QP algorithm that is initialized with an SOCP relaxation. However these multi-period OPF formulations neglect the non-unity charge and discharge efficiency of the battery, which can create unrealizable solutions to the OPF problem in the form of simultaneous charging and discharging of the battery.

- In this paper, the authors present a novel hierarchical OPF scheme for distribution systems operations that separates out the slow mechanical (into a discrete control scheme) and fast power-electronic (into a continuous control scheme) grid assets on two different timescales.
- For the continuous control scheme, the Service Transformer Layer (STL) elements are dispatched optimally using multi-period three-phase SOCP convex relaxation techniques applied to radial distribution networks for fast corrective control.
- The phenomenon of simultaneous charging and discharging of batteries in a convex model of 3-phase system is also analyzed and conditions are provided under which this can be avoided.

The rest of the paper is organized as follows. Section II provides the MILP formulation of the outer loop to optimize the operation of mechanical control assets. Section III provides the convex formulation of the inner loop to reduce the distribution network losses. Conditions under which the complementarity constraint is enforced in the convex formulation of the inner loop are analyzed in Section IV. Test case results on the IEEE-13 bus system are presented in Section V and finally the conclusions and future work are presented in Section VI.

II. OUTER LOOP FORMULATION: VOLTAGE POSITIONING

The outer loop of the formulation is designed to operate the discrete control assets of the distribution network like on-load tap change transformers, capacitor banks, etc. Since these devices operate by mechanical switching, to reduce wear and
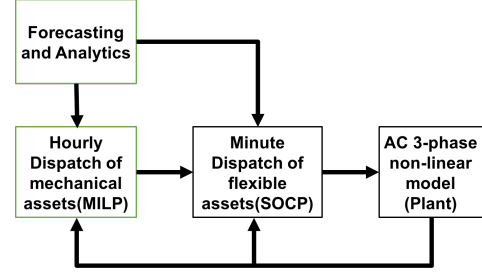

Figure 1. Flowchart showing the hierarchical time-scale control algorithm. Based on the hourly forecast net load, the MILP model dispatches the mechanical assets. Fixing the mechanical assets and based on minute by minute net load forecasts, the SOCP model determines the dispatch of STL flexible resources. The control inputs are then fed to a 3-phase non-linear model of the system.

tear, their values are updated at a slower time scale of the order of an hour. In this optimization loop, the aim is to minimize the voltage deviation from a nominal set-point using the operation of these discrete assets. In addition to scheduling mechanical assets, the outer loop also positions energy of the STL elements (i.e., schedules active power exchanges) to take into account the variability of solar PV generation and forecast energy demands (and, possibly, energy market interactions). Note that the reactive capability of STL elements is reserved for corrective control in the inner loop.

Since discrete decision variables only take integer values, the outer loop problem turns into a mixed-integer problem, which is NP-hard. Branch and bound techniques can be effective on mixed-integer programs if their continuous versions are convex. In order to reduce the computational complexity of the outer loop, a three-phase linearized model of the network is used and the problem is reduced to a mixed-integer linear program (MILP) [13]. This problem is solved in a receding horizon fashion where the 24 hr ahead solar and load forecasts are used to obtain the operation of discrete assets.

For the model, consider an unbalanced three-phase network with N nodes and L feeder segments, where each node and segment has $\phi = 1, 2, 3$ phases. The system has an STL element at nodes $G \subset N$, transformers between nodes on segments $T \subset L$ and capacitor banks at nodes $C \subset N$. The STL elements are composed of distributed generation, such as solar PV and battery storage as shown in figure 2. These STL elements are capable of four quadrant operation (i.e., can supply and/or consume active and reactive power). The optimization horizon runs from $k = 1, ..., K - 1, K$.

Let $U_{n,k} \in \mathbb{R}^{|\phi|}$ represent the square of the per unit voltage magnitude at node n at time instant k (i.e., $U_{n,k} = |V_{n,k}|^2$) and $U_{\text{nom},n} \in \mathbb{R}^{|\phi|}$ represent the square of the per unit nominal voltage magnitude at node n. The MILP problem is then formulated as:

$$\min \sum_{k=k_o}^{K} \sum_{\phi=1}^{|\phi|} \sum_{n=1}^{N} (U_{n,k} - U_{\text{nom},n})^2 \qquad (1)$$

subject to: **Power balance (neglecting losses):**

$$P_{n,k} = \sum_{m} P_{m,k} + P_{n,k}^L - W_{n,k}^N, \forall n \in G, k \qquad (2)$$

$$P_{n,k} = \sum_m P_{m,k} + P_{n,k}^L, \forall n \in N/G, k \quad (3)$$

$$Q_{n,k} = \sum_m Q_{m,k} + Q_{n,k}^L - \xi_{n,k} U_{n,k} q_{nom,n}, \forall n \in C, k \quad (4)$$

$$Q_{n,k} = \sum_m Q_{m,k} + Q_{n,k}^L, \forall n \in N/C, k \quad (5)$$

where $S_{n,k} = P_{n,k} + jQ_{n,k} \in \mathbb{C}^{|\phi|}$ is the complex power at node n at time k, $S_{n,k}^L = P_{n,k}^L + jQ_{n,k}^L \in \mathbb{C}^{|\phi|}$ is the complex load at node n at time k, $W_{n,k}^N \in \mathbb{C}^{|\phi|}$ is the STL generated power at node n at time k, $\xi_{n,k} \in \mathbb{Z}^{|\phi|}$ is the number of capacitor banks operated at node n at time k and $q_{nom,n} \in \mathbb{R}^{|\phi|}$ is the nominal ratings of each capacitor bank connected at node n.

Voltage square magnitude relation (neglecting losses):

$$U_{n,k} = U_{m,k} + M_{n,m}^P P_{m,k} + M_{n,m}^Q Q_{m,k}, \forall n \in N/T, k \quad (6)$$

$$U_{n,k} = (1 + \tau_n \zeta_{n,k})^2 U_{m,k}, \forall n \in T, k \quad (7)$$

where $M_{n,m}^P \in \mathbb{R}^{|\phi| \times |\phi|}$ and $M_{n,m}^Q \in \mathbb{R}^{|\phi| \times |\phi|}$ are obtained from the impedance matrices of the feeder segments [13] connecting nodes n and m, $\tau_n \in \mathbb{R}^{|\phi|}$ is the tap step at node n and $\zeta_{n,k} \in \mathbb{Z}^{|\phi|}$ is the integer representing the tap positions of the transformer at node n and time k.

Voltage square magnitude constraint:

$$U_{min,n} \le U_{n,k} \le U_{max,n}, \forall n \in N, k \quad (8)$$

where $U_{min,n} \in \mathbb{R}^{|\phi|}$ and $U_{max,n} \in \mathbb{R}^{|\phi|}$ represent the minimum and maximum allowable voltage magnitude square at node n and time k.

Substation voltage set-point:

$$U_{0,k} = y_{nom}, \forall k \quad (9)$$

where $y_{nom} \in \mathbb{R}^{|\phi|}$ is the fixed feeder voltage

Line power flow constraint:

$$P_{n,k}^2 + Q_{n,k}^2 \le S_{max,n}^2, \forall n \in N, k \quad (10)$$

where $S_{max,n} \in \mathbb{R}^{|\phi|}$ is the maximum allowable complex power flowing into node n.

Node power relations:

$$W_{n,k}^N = W_{n,k}^S + P_{n,k}^d - P_{n,k}^c, \forall n \in G, k \quad (11)$$

where $W_{n,k}^S \in \mathbb{C}^{|\phi|}$ is the solar power generated at node n and time k, $P_{n,k}^d \in \mathbb{R}^{|\phi|}$ and $P_{n,k}^c \in \mathbb{R}^{|\phi|}$ are the battery discharge and charge power respectively at node n and time k.

Battery state of charge and complementarity constraints:

$$B_{n,k+1} = B_{n,k} + \eta_{c,n} P_{n,k}^c \Delta t - \frac{P_{n,k}^d}{\eta_{d,n}} \Delta t, \forall n \in G, k \quad (12)$$

$$B_{min,n} \le B_{n,k} \le B_{max,n}, \forall n \in G, k \quad (13)$$

$$z_{n,k} P_{max,n} \ge P_{n,k}^c \ge 0, \forall n \in G, k \quad (14)$$

$$(1 - z_{n,k}) P_{max,n} \ge P_{n,k}^d \ge 0, \forall n \in G, k \quad (15)$$

$$z_{n,k} \in {0, 1}, \forall n \in G, k \quad (16)$$

where $B_{n,k} \in \mathbb{R}^{|\phi|}$ is the state of charge of the battery at node n and time k, $\eta_{c,n} \in \mathbb{R}^{|\phi|}$ and $\eta_{d,n} \in \mathbb{R}^{|\phi|}$ are the charging and discharging efficiencies respectively at node n,

$B_{min,n} \in \mathbb{R}^{|\phi|}$ and $B_{max,n} \in \mathbb{R}^{|\phi|}$ are the minimum and maximum state of charge of the batteries at node n, $P_{max,n} \in \mathbb{R}^{|\phi|}$ is the maximum allowable power from the battery at node n, $z_{n,k} \in \mathbb{Z}^{|\phi|}$ is either 0 or 1, and $\Delta t \in \mathbb{R}$ is the time between two intervals k and $k + 1$.

Transformer tap and Capacitor bank constraint:

$$N_{max,n} \ge \zeta_{n,k} \ge N_{min,n}, \forall n \in T, k \quad (17)$$

$$Q_{max,n} \ge q_{n,k}^t \ge Q_{min,n}, \forall n \in C, k \quad (18)$$

where $N_{min,n} \in \mathbb{Z}^{|\phi|}$ and $N_{max,n} \in \mathbb{Z}^{|\phi|}$ are the minimum and maximum allowable tap positions of the transformer at node n, $Q_{min,n} \in \mathbb{Z}^{|\phi|}$ and $Q_{max,n} \in \mathbb{Z}^{|\phi|}$ are the minimum and maximum number of allowable capacitor banks that can be used at node n.

The mixed-integer program given in (1)-(18) is non-linear due to the capacitor bank and transformer tap relations in (4) and (7). The capacitor bank relation of (4) is linearized by using McCormick relaxation [22]:

$$Q_{n,k} = \sum_m Q_{m,k} + Q_{n,k}^L - q_{n,k} q_{nom,n}, \forall n \in C, k \quad (19)$$

$$q_{n,k} \ge U_{n,k} Q_{min,n} + q_{n,k}^t U_{min,n} - Q_{min,n} U_{min,n} \quad (20)$$

$$q_{n,k} \ge U_{n,k} Q_{max,n} + q_{n,k}^t U_{max,n} - Q_{max,n} U_{max,n} \quad (21)$$

$$q_{n,k} \le U_{n,k} Q_{max,n} + q_{n,k}^t U_{min,n} - Q_{max,n} U_{min,n} \quad (22)$$

$$q_{n,k} \le U_{n,k} Q_{min,n} + q_{n,k}^t U_{max,n} - Q_{min,n} U_{max,n} \quad (23)$$

where $q_{n,k} \in \mathbb{R}^{|\phi|}$

The non-linear transformer tap relation in (7) is first linearized as in [16] by neglecting the quadratic term.

$$U_{n,k} = U_{m,k} + 2\tau_n x_{n,t}, \forall n \in T, k \quad (24)$$

The modeling error is no worse than about ± 1 tap position. Then a similar McCormick relaxation is applied. With these changes, the outer loop problem is simplified to a mixed-integer linear program (MILP)

III. INNER LOOP FORMULATION: CORRECTIVE OPF

The aim of the inner loop is to minimize the real power losses in the distribution network and track a power reference signal from the transmission level, while keeping the system within its operational bounds. This program optimizes the Service Transformer Layer (STL) elements, over the fast timescale.
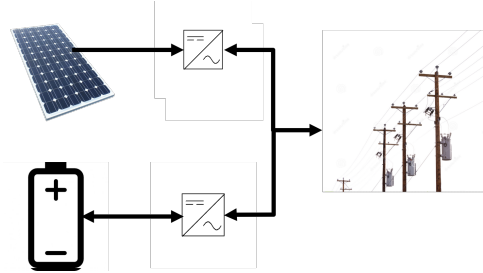

Figure 2. Service Transformer Layer (STL) architecture. The STL elements are controlled through a four quadrant control scheme and can supply and consume both real and reactive power. Each STL element is composed of a renewable source of energy such as solar power and some form of storage like a battery bank.

This corrective optimization loop is required to be fast (order of a minute). A three-phase second order cone program (SOCP) is used to solve the optimization problem. SOCP's are numerically more robust than SDP's and also have a shorter solve time. A branch flow model (BFM) is used to represent the power flow equations of the three-phase network. Branch flow models are generally more numerically robust then branch injection models (BIM) [18]. Thus, let BFM be defined as:

$$\begin{bmatrix} W_{n,t} & S_{l,t} \\ S_{l,t}^H & I_{l,t} \end{bmatrix} = \begin{bmatrix} V_{n,t} \\ i_{l,t} \end{bmatrix} \begin{bmatrix} V_{n,t} \\ i_{l,t} \end{bmatrix}^H \quad (25)$$

where $V_{n,t} \in \mathbb{C}^{|\phi|}$ is the voltage at node n and time t, $i_{l,t} \in \mathbb{C}^{|\phi|}$ is the current in line l at time t.

The inner loop optimization problem can then be formulated as:

$$\min \sum_{t=t_0}^{T} \sum_{\phi=1}^{|\phi|} (diag(S_{0,t})) + \sum_{l=1}^{L} \sum_{t=t_0}^{T} \sum_{\phi=1}^{|\phi|} (diag(R_l I_{l,t})) \quad (26)$$

subject to:

Power balance (BFM):

$$diag(S_{l,t}) - diag(Z_l I_{l,t}) + W_{n,t}^N - S_{n,t}^L = \sum_p (diag(S_{p,t})) \quad (27)$$

where $R_l \in \mathbb{R}^{|\phi| \times |\phi|}$ is the resistance of line l and $Z_l \in \mathbb{C}^{|\phi| \times |\phi|}$ is the impedance of line l.

Power flow equations(BFM):

$$W_{n,t} = W_{m,t} - (S_{l,t} Z_l' + Z_l S_{l,t}) + Z_l I_{l,t} Z_l' \quad (28)$$

Line power flow constraints:

$$|diag(S_{l,t})| \le S_{max,n}, \forall l, t \quad (29)$$

Relation between $W_{n,t}, I_{l,t}, S_{l,t}$ and $V_{n,t}, i_{n,t}$ is then:

$$|W_{n,t}(i,j)|^2 = W_{n,t}(i,i)W_{n,t}(j,j), \forall i \ne j \quad (30)$$

$$|I_{l,t}(i,j)|^2 = I_{l,t}(i,i)I_{l,t}(j,j), \forall i \ne j \quad (31)$$

$$|S_{l,t}(i,j)|^2 = W_{n,t}(i,i)I_{l,t}(j,j), \forall i,j \quad (32)$$

Voltage constraint:

$$U_{min,n} \le diag(W_{i,t}) \le U_{max,n}, \forall n \in N, t \quad (33)$$

Solar PV constraint:

$$|W_{n,t}^S| \le G_{max,n}, \forall n \in G, t \quad (34)$$

where $G_{max,n} \in \mathbb{R}^{|\phi|}$ is the apparent power limit of the solar inverter at node n.

Node power relations:

$$real(W_{n,t}^N) = real(W_{n,t}^S) + P_{n,t}^d - P_{n,t}^c \quad (35)$$

$$imag(W_{n,t}^N) = imag(W_{n,t}^S) + P_{n,t}^q \quad (36)$$

where $P_{n,t}^q \in \mathbb{R}^{|\phi|}$ is the reactive power supplied by the battery at node n and time t.

Battery state of charge and complementarity constraints:

$$(P_{n,t}^d - P_{n,t}^c)^2 + (P_{n,t}^q)^2 \le H_{max,n}^2 \quad (37)$$

$$B_{n,t+1} = B_{n,t} + \eta_{c,n} P_{n,t}^c \Delta t - \frac{P_{n,t}^d}{\eta_{d,n}} \Delta t \quad (38)$$

$$B_{min,n} \le B_{n,t} \le B_{max,n} \quad (39)$$

$$z_{n,t} P_{max,n} \ge P_{n,t}^d \ge 0 \quad (40)$$

$$(1 - z_{n,t}) P_{max,n} \ge P_{n,t}^c \ge 0 \quad (41)$$

$$z_{n,t} \in \mathbf{0, 1} \quad (42)$$

where $H_{max,n} \in \mathbb{R}^{|\phi|}$ is the apparent power limit of the battery inverter at node n.

The inner loop model from (26)-(42) is non-linear due to the equality constraints in (30)-(32) and also mixed-integer due to the integer constraints in (40)-(42). These constraints make the problem NP-hard. The non-linear equality constraints in (30)-(32) are relaxed by a second order cone relaxation to convert the problem into an SOCP, as shown below:

$$\left| \begin{matrix} 2W_{n,t}(i,j) \\ W_{n,t}(i,i) - W_{n,t}(j,j) \end{matrix} \right|_2 \le W_{n,t}(i,i) + W_{n,t}(j,j) \quad (43)$$

$$\left| \begin{matrix} 2I_{l,t}(i,j) \\ I_{l,t}(i,i) - I_{l,t}(j,j) \end{matrix} \right|_2 \le I_{l,t}(i,i) + I_{l,t}(j,j) \quad (44)$$

$$\left| \begin{matrix} 2S_{l,t}(i,j) \\ W_{n,t}(i,i) - I_{l,t}(j,j) \end{matrix} \right|_2 \le W_{n,t}(i,i) + I_{l,t}(j,j) \quad (45)$$

If the complementarity constraints in (40)-(42) are also relaxed, the inner loop model becomes convex and can be solved in polynomial time.

IV. RELAXING COMPLEMENTARITY CONSTRAINT

The constraints in (40)-(42) ensure that the batteries in the system do not simultaneously charge and discharge. But these constraints make the second order cone program of the inner loop non-convex. One solution to this problem would be the use of mixed-integer SOCP as in the outer loop, but this would increase the computation time substantially. As it is desired for the inner loop to solve to (near) optimality within a minute, this option would not be realizable. Thus, the approach is to relax these constraints and analyze under which conditions the optimal solution satisfies the complementarity constraint.

In [23], [24], the authors provide conditions under which simultaneous charging and discharging can be avoided in the optimal solution for an economic dispatch problem. In [24], Karush-Kuhn-Tucker (KKT) conditions are analyzed for a linear DC model of the economic dispatch problem and they show that under realistic assumptions simultaneous charging and discharging is avoided. In this paper, this analysis is extended to a distribution system setting where the objective is to minimize the network losses and also consider four-quadrant battery operation.

A. Without penalizing SoC deviations from reference

Without the complementarity constraints in the SOCP model, simulations in Fig. 3 clearly illustrate simultaneous charging and discharging for battery connected at node 680 and phase b in the test feeder in Fig. 4 for the IEEE-13 node system [25]. To overcome this battery modeling challenge, the objective function of the optimization problem (network objective) is modified to include a term that accounts for the losses in the battery due to charging and discharging effects. Since simultaneous charging and discharging results in

higher battery losses, the addition of this term in the objective function overcomes the effect.

The addition of this battery power loss term in the objective function does not affect the original network loss function. The solutions have the same objective value and the battery loss term restricts the feasible set to points that also enforce the complementarity constraint. This is an improvement from the standard method of avoiding simultaneous charging and discharging by explicitly adding the battery power into the objective function [26], which does mitigate the charging issue, but yields a sub-optimal solution.

The modified objective function is given by:

$$\mathcal{F}(\mathcal{N}) + \sum_{t=t_0}^{T} \sum_{n=1}^{|G|} \sum_{\phi=1}^{|\phi|} P_{n,t}^c(1 - \eta_{c,n}) + P_{n,t}^d\left(\frac{1}{\eta_{d,n}} - 1\right) \quad (46)$$

where $\mathcal{F}(\mathcal{N})$ is given in (26) and the second terms minimize the power losses due to battery inefficiency. The state of charge tracking is removed from the objective and its effect will be analyzed in the next section. With the modified objective function, the SOCP optimization satisfies the complementarity condition as shown in Fig. 3. Lemma IV.1 provides conditions under which the inner loop SOCP enforces the battery's complementarity constraints and avoids simultaneous charging and discharging.
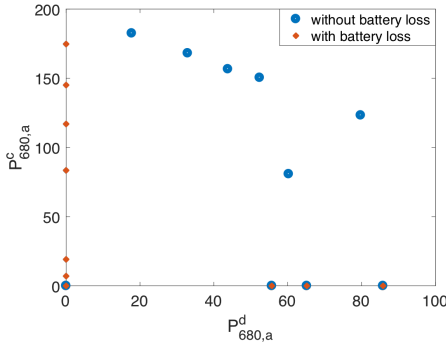

Figure 3. Comparison of simultaneous charge and discharge in battery at node 680, phase a with and without battery loss term in objective. The reason for simultaneous occurrence of charge and discharge is that the objective function only has terms for the losses in the distribution lines and does not take into account the losses in the battery due to charging and discharging (this is different from [24] where the cost explicitly includes terms for battery power). Thus, all solutions with the same value for $P^d - P^c$, are equivalent in the optimization solution, which begets simultaneous charging and discharging.

Lemma IV.1. *Since the SOCP optimization problem is convex and Slater's condition holds, the Karush-Kuhn-Tucker (KKT) conditions are both necessary and sufficient. It can be proven that the relaxation is exact under the following sufficient conditions:*

C1: $\lambda_p \geq 0$ (next unit of power injected will not decrease overall losses)

C2: $\lambda_s = 0$ (STL element is not operating at its apparent power limt, i.e., inverter is oversized)

where λ_p is the Lagrange multiplier associated with (27) and λ_s is the Lagrange multiplier associated with (37).

Proof. From the KKT conditions, the following equation is obtained with respect to battery charging power at node n, phase ϕ at time t:

$$\frac{\partial L}{\partial P^c} = (1 - \eta_c) - \underline{\lambda_c} + \overline{\lambda_c} - \eta_c \Gamma(t)\Delta t \\ + \lambda_p - 2\lambda_s(P^d - P^c) = 0 \quad (47)$$

where L is the Lagrangian, $\Gamma(t) = \sum_{\tau=t}^{T}(\beta_{1,n,\phi}(\tau) - \beta_{2,n,\phi}(\tau))$, $\beta_{1,n,\phi}(\tau)$ and $\beta_{2,n,\phi}(\tau)$ are Lagrange multipliers associated with (39), P^c and P^d are the charging and discharging power for the battery at node n, phase ϕ at time t and η_c is the charging efficiency of the battery at node n. Let $P^c > 0$, then $\underline{\lambda_c} = 0$. Using C1, C2 and that $\eta_c < 1$, then all other terms in (47) are non-negative which results in $\Gamma(t) > 0$. With respect to the battery discharge power, the following KKT condition results:

$$\frac{\partial L}{\partial P^d} = \left(\frac{1}{\eta_d} - 1\right) - \underline{\lambda_d} + \overline{\lambda_d} + \frac{\Gamma(t)\Delta t}{\eta_d} \\ - \lambda_p + 2\lambda_s(P^d - P^c) = 0 \quad (48)$$

Assume $P^d > 0$ (simultaneous charge and discharge), then $\underline{\lambda_d} = 0$. Adding (47) and (48) gives:

$$\left(\frac{1}{\eta_d} - \eta_c\right) + \overline{\lambda_c} + \overline{\lambda_d} + \Gamma(t)\Delta t \left(\frac{1}{\eta_d} - \eta_c\right) = 0 \quad (49)$$

In the above equation $\overline{\lambda_c} \geq 0$ and $\overline{\lambda_d} \geq 0$, which implies $\Gamma(t) < 0$. But this is contradiction, which shows that $P^c P^d \equiv 0$. Case for $P^d > 0$ is similar. □

B. Terminal penalty on state of charge (SoC)

When the reference SoC (provided by the outer loop MILP) tracking is added to the objective of the inner loop SOCP, the objective function of the SOCP becomes:

$$\mathcal{F}(\mathcal{N}) + \alpha \sum_{t=t_0}^{T} \sum_{n=1}^{|G|} \sum_{\phi=1}^{|\phi|} \left(P_{n,t}^c(1 - \eta_{c,n}) + P_{n,t}^d(\frac{1}{\eta_{d,n}} - 1) \right) \\ + \gamma \sum_{n=1}^{|G|} \sum_{\phi=1}^{|\phi|} \left(\Delta B_n\right)^2 \quad (50)$$

where $\Delta B_n = B_{n,T} - B^{ref}$, $B_{n,T}$ is the terminal SoC of the battery at the terminal interval T given by:

$$B_{n,T}(\phi) = \Delta t \sum_{t=t_0}^{T} \eta_{c,n} P_{n,t}^c(\phi) - \frac{P_{n,t}^d(\phi)}{\eta_{d,n}} \quad (51)$$

and B^{ref} is the reference SoC obtained from solving the outer loop MILP. The optimal solution will now have a Pareto-optimal front between the loss reduction term and the SoC tracking term. It is necessary to check whether the complementarity constraint holds under this addition to the objective function and Lemma IV.2 provides the sufficient conditions under which the complementarity condition is satisfied.

Lemma IV.2. *With reference tracking, the complementarity constraint is enforced under these sufficient conditions:*

C1: $\lambda_p \geq 0$

C2: $\lambda_s = 0$

C3: $\alpha > 0$

Proof. Using (51), the KKT condition with respect to the battery charging power gives:

$$\frac{\partial L}{\partial P^c} = \alpha(1 - \eta_c) + 2\gamma\eta_c \Delta B_n(\phi)\Delta t - \underline{\lambda_c} + \overline{\lambda_c}$$
$$- \eta_c\Gamma(t)\Delta t + \lambda_p - 2\lambda_s(P^d - P^c) = 0 \quad (52)$$

Let $P^c > 0$, then $\underline{\lambda_c} = 0$, $\overline{\lambda_c} \geq 0$, and (52) gives:

$$(\Gamma(t) - 2\gamma\Delta B_n(\phi))\Delta t \geq \frac{\alpha(1-\eta_c)}{\eta_c} + \frac{\lambda_p}{\eta_c}$$
$$+ \frac{2\lambda_s(P^c - P^d)}{\eta_c} \quad (53)$$

The KKT condition with respect to the battery discharge power gives:

$$\frac{\partial L}{\partial P^d} = \alpha(\frac{1}{\eta_d} - 1) - 2\frac{\gamma}{\eta_d}(B_{n,T} - B^{ref}) - \underline{\lambda_d} + \overline{\lambda_d}$$
$$+ \Gamma(t)\frac{\Delta t}{\eta_d} - \lambda_p + 2\lambda_s(P^d - P^c) = 0 \quad (54)$$

Since $\overline{\lambda_d} \geq 0$, (54) gives:

$$(\Gamma(t) - 2\gamma\Delta B_n(\phi))\Delta t \leq -\alpha(1 - \eta_d) + \eta_d\underline{\lambda_d} + \eta_d\lambda_p$$
$$+ 2\eta_d\lambda_s(P^c - P^d) \quad (55)$$

Comparing (53) and (55) gives:

$$\underline{\lambda_d}\frac{\eta_c\eta_d}{1 - \eta_c\eta_d} \geq \alpha + \lambda_p + 2\lambda_s(P^c - P^d) \quad (56)$$

Provided $\eta_c\eta_d \neq 1$, under conditions C1, C2 and C3, given above, (56) provides: $\underline{\lambda_d} > 0$, which proves that under the given sufficient conditions, when $P^c > 0$, then $P^d = 0$. A similar procedure can be used to show that when $P^d > 0$, then $P^c = 0$. Hence, $P^d P^c \equiv 0$ is enforced. $\square$

V. TEST CASES AND NUMERICAL SIMULATIONS

Test simulations are conducted on the IEEE-13 node distribution system [25], which is an unbalanced three-phase system consisting of one, two and three phase lines. The switch between nodes 671 and 692 is assumed to be closed at all times. The system has a three-phase OLTC transformer between nodes 633 and 634. Capacitor banks are placed at nodes 675 and 611. The system is modified to include STL elements at nodes 632, 675, 680 and 684 as shown in Fig. 4. These elements consist of solar PV generation plus equivalent battery bank and are capable of four quadrant operation.
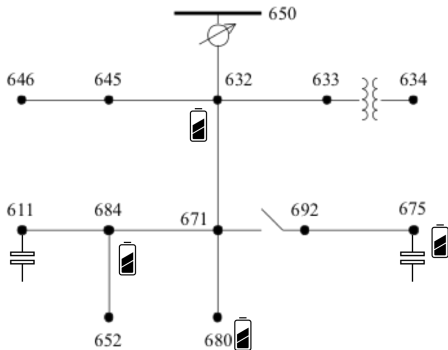

Figure 4. IEEE 13 node test feeder used as a test case

A. Test case results

The control inputs obtained from the outer and inner loop of the optimization algorithm for a given solar and load profile are applied to the IEEE-13 node system. From the output of the system as shown in Fig. 5, it can be seen that the voltages are well tracked and are within their bounds and the battery state of charge is accurately tracked. From the results in Figure 5, it appears that the SOCP voltages upper bound the plant voltage. However, this relationship breaks down when the batteries hit their limits, in which case the order can reverse. Future work will establish conditions under which this upper bound is upheld.
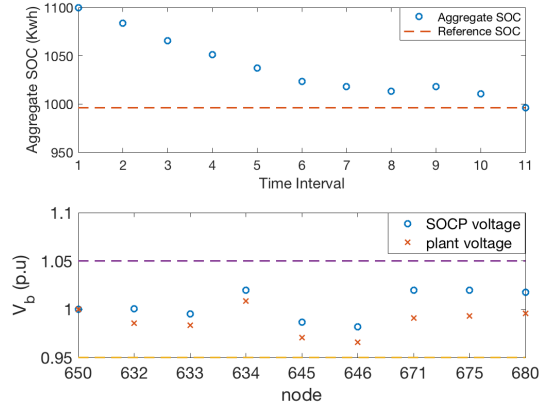

Figure 5. (a) Tracking of the reference SoC by the aggregate SoC of the network batteries. The batteries discharge power at each interval to meet the power demand and finally reach the reference SoC level provided by the outer loop MILP. (b) Comparison of voltage profile at phase b between the SOCP model and the 3-phase plant model using forward-backward sweep.

B. Improvement in system performance with flexible resources

Two cases of multi-period OPF are run, one with storage devices and one without and the effect on total network losses is compared. The comparison is shown in Fig. 6(a). Figure 6(b) shows how the network losses change with increase in battery capacity.

VI. CONCLUSIONS AND FUTURE WORK

This paper presents a technique to optimally solve an unbalanced three-phase distribution network by optimizing the slow and fast control assets over different time scales using multi-period optimal power flow techniques. A multi-period mixed-integer linear program solves the OPF for the slow mechanical assets and a multi-period SOCP is used to solve the optimization for the fast STL elements.

The complementarity constraint problem for the battery model is studied and sufficient conditions are provided under which the complementarity constraint condition is satisfied at optimality for the convex SOCP problem. The effectiveness of these algorithms is tested on a three-phase non-linear model of IEEE-13 node system. Further analysis on the model shows how storage flexibility in the system improves performance and reduces losses.
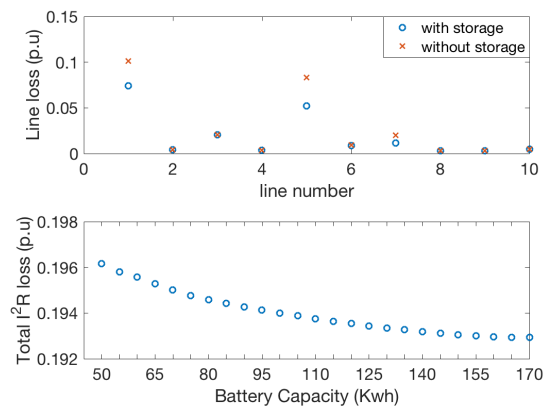
Figure 6. (a) Comparison of losses at different lines in the network between storage and without storage MOPF. From the figure it can be seen that there is a reduction in the network losses with the inclusion of storage especially in line connecting nodes 650 and 632 and 632 and 671. The battery connected at node 632 minimizes the power required to be sent across these lines which reduces the losses. (b) Change in total predicted network loss with increase in storage capacity. There is a particular amount of storage beyond which addition of more storage to the network has negligible effect on the loss reduction. For this test case, the value is around 150 kWh.

Future work will analyze the three-phase SOCP relaxation and find necessary conditions under which it is tight. Improving the coupling between inner and outer layers as it relates to market conditions and relate closed-loop performance of inner loop to required available flexibility and measurements, is also a future scope for improvement. Testing the proposed techniques on large-scale networks using distributed algorithms, which reduce the computation time, will also be completed. Future work will also concentrate on improving and relaxing the complementarity conditions provided in *Lemmas* IV.1 and IV.2.

REFERENCES

[1] J. Singer, *Enabling Tomorrow's Electricity System: Report of the Ontario Smart Grid Forum*. Independent Electricity System Operator, 2010.

[2] T. Ackermann, T. Prevost, V. Vittal, A. J. Roscoe, J. Matevosyan, and N. Miller, "Paving the way: A future without inertia is closer than you think," *IEEE Power and Energy Magazine*, vol. 15, no. 6, pp. 61–69, 2017.

[3] M. Baran and F. F. Wu, "Optimal sizing of capacitors placed on a radial distribution system," *IEEE Transactions on power Delivery*, vol. 4, no. 1, pp. 735–743, 1989.

[4] F. Katiraei, C. Sun, and B. Enayati, "No inverter left behind: protection, controls, and testing for high penetrations of pv inverters on distribution systems," *IEEE Power and Energy Magazine*, vol. 13, no. 2, pp. 43–49, 2015.

[5] S. Paudyal, C. A. Canizares, and K. Bhattacharya, "Three-phase distribution opf in smart grids: Optimality versus computational burden," *Innovative Smart Grid Technologies (ISGT Europe), 2nd IEEE PES International Conference and Exhibition on*, 2011.

[6] R. Arghandeh and R. Broadwater, "Distributed energy storage control for optimal adoption of solar energy in residential networks," *ASME 2012 Power Conference, Anaheim CA, USA*, vol. 3, 2012.

[7] I. A. Hiskens and R. J. Davy, "Exploring the power flow solution space boundary," *IEEE Transactions on Power Systems*, vol. 16, no. 3, pp. 389–395, 2001.

[8] J. Lavaei and S. H. Low, "Zero duality gap in optimal power flow problem," *IEEE Transactions on Power Systems*, vol. 27, no. 1, pp. 92–107, 2012.

[9] J. Lavaei, D. Tse, and B. Zhang, "Geometry of power flows and optimization in distribution networks," *IEEE Transactions on Power Systems*, vol. 29, no. 2, pp. 572–583, 2014.

[10] R. A. Jabr, "Radial distribution load flow using conic programming," *IEEE Transactions on Power Systems*, vol. 21, no. 3, pp. 1458–1459, 2006.

[11] M. Farivar, C. R. Clarke, S. H. Low, and K. M. Chandy, "Inverter var control for distribution systems with renewables," *Smart Grid Communications (SmartGridComm), IEEE International Conference on*, pp. 457–462, 2011.

[12] P. Roux, Y.-L. Voronin, and S. Sankaranarayanan, "Validating numerical semidefinite programming solvers for polynomial invariants," *International Static Analysis Symposium*, pp. 424–446, 2016.

[13] M. D. Sankur, R. Dobbe, E. Stewart, D. S. Callaway, and D. B. Arnold, "A linearized power flow model for optimization in unbalanced distribution systems," *arXiv preprint arXiv:1606.04492*, 2016.

[14] B. A. Robbins and A. D. Domínguez-García, "Optimal reactive power dispatch for voltage regulation in unbalanced distribution systems," *IEEE Transactions on Power Systems*, vol. 31, no. 4, pp. 2903–2913, 2016.

[15] B. A. Robbins, H. Zhu, and A. D. Domínguez-García, "Optimal tap setting of voltage regulation transformers in unbalanced distribution systems," *IEEE Transactions on Power Systems*, vol. 31, no. 1, pp. 256–267, 2016.

[16] E. Briglia, S. Alaggia, and F. Paganini, "Distribution network management based on optimal power flow: Integration of discrete decision variables," *Information Sciences and Systems (CISS), 51st Annual Conference on*, pp. 1–6, 2017.

[17] E. Dall'Anese, H. Zhu, and G. B. Giannakis, "Distributed optimal power flow for smart microgrids," *IEEE Transactions on Smart Grid*, vol. 4, no. 3, pp. 1464–1475, 2013.

[18] L. Gan and S. H. Low, "Convex relaxations and linear approximation for optimal power flow in multiphase radial networks," *Power Systems Computation Conference (PSCC)*, pp. 1–9, 2014.

[19] D. Gayme and U. Topcu, "Optimal power flow with large-scale storage integration," *IEEE Transactions on Power Systems*, vol. 28, no. 2, pp. 709–717, 2013.

[20] A. Gopalakrishnan, A. U. Raghunathan, D. Nikovski, and L. T. Biegler, "Global optimization of multi-period optimal power flow," *American Control Conference*, pp. 1157–1164, 2013.

[21] J. F. Marley, D. K. Molzahn, and I. A. Hiskens, "Solving multiperiod opf problems using an AC-QP algorithm initialized with an SOCP relaxation," *IEEE Transactions on Power Systems*, vol. 32, no. 5, pp. 3538–3548, 2017.

[22] G. P. McCormick, "Computability of global solutions to factorable nonconvex programs: Part I—convex underestimating problems," *Mathematical programming*, vol. 10, no. 1, pp. 147–175, 1976.

[23] M. R. Almassalkhi and I. A. Hiskens, "Model-predictive cascade mitigation in electric power systems with storage and renewables—part I: Theory and implementation," *IEEE Transactions on Power Systems*, vol. 30, no. 1, pp. 67–77, 2015.

[24] Z. Li, Q. Guo, H. Sun, and J. Wang, "Sufficient conditions for exact relaxation of complementarity constraints for storage-concerned economic dispatch," *IEEE Transactions on Power Systems*, vol. 31, no. 2, pp. 1653–1654, 2016.

[25] W. H. Kersting, "Radial distribution test feeders," *Power Engineering Society Winter Meeting*, vol. 2, pp. 908–912, 2001.

[26] C. Shao, X. Wang, X. Wang, C. Du, C. Dang, and S. Liu, "Cooperative dispatch of wind generation and electric vehicles with battery storage capacity constraints in scuc," *IEEE Transactions on Smart Grid*, vol. 5, no. 5, pp. 2219–2226, 2014.